Derived methane in the stratosphere and lower mesosphere from Aura Microwave Limb Sounder measurements of nitrous oxide, water vapor, and carbon monoxide

K. Minschwaner · G. L. Manney

Abstract The global distribution of methane (CH_4) in the stratosphere and lower mesosphere has been derived using coincident measurements of water vapor (H_2O), carbon monoxide (CO), and nitrous oxide (N_2O) from the Microwave Limb Sounder (MLS) instrument on the Aura satellite. The derivation method is based on empirical relationships between these species established using observations from the Atmospheric Chemistry Experiment—Fourier Transform Spectrometer (ACE-FTS) on the SCISAT I satellite. The observed correlation between CH_4 and N_2O from ACE-FTS is used to derive CH_4 from MLS measurements of N_2O in the lower stratosphere, extending from a pressure of 100 hPa to a range of 30–10 hPa, depending on atmospheric conditions. In the upper stratosphere and lower mesosphere, between 30–10 hPa and 0.1 hPa, correlations between CH_4 and H_2O are used to derive CH_4 from MLS measurements of H_2O. Coincident MLS measurements of CO are utilized to separate two distinct air mass regimes in the CH_4 - H_2O relationship. This new methane data set covers all seasons and latitudes observed by MLS over the course of the Aura mission from 2004 to 2014. Examples are shown demonstrating the consistency of MLS derived CH_4 with other trace gas measurements.

Keywords Methane · Stratosphere · MLS · ACE-FTS

1 Introduction

The amount of methane (CH_4) in the atmosphere has increased from a preindustrial range of 400–700 ppbv to the present level of ~1800 ppbv, and its infrared radiative forcing of climate now ranks second among all of the long lived greenhouse gases (Myhre et al. 2013). In the stratosphere, methane represents one of the largest chemical sources for hydrogen-containing species such as water vapor (e.g., Wrotny et al. 2010), which itself is an important greenhouse gas in the stratosphere (e.g., Solomon et al. 2010).

K. Minschwaner (✉) · G. L. Manney
Department of Physics, New Mexico Institute of Mining and Technology, Socorro, NM, USA
e-mail: krm@kestrel.nmt.edu

G. L. Manney
NorthWest Research Associates, Socorro, NM, USA

The local lifetime of CH_4 in the atmosphere varies dramatically with latitude, season, and altitude. In the troposphere, the global average lifetime is on the order of 10 years, resulting primarily from destruction through reactions with hydroxyl (OH) (SPARC 2013). At higher altitudes, most of the CH_4 enters the stratosphere through the upward branch of the Brewer-Dobson circulation at low latitudes and is subsequently destroyed by reactions with both OH and excited state atomic oxygen ($O(^1D)$) in the stratosphere, and by photodissociation at Lyman-alpha wavelengths (~121 nm) in the mesosphere. The mean stratospheric lifetime of CH_4 is between 84 and 103 years based on an analysis of its observed correlation with CFC-11 in the lower stratosphere (Volk et al. 1997). This spread in values arises from the range of lifetimes assumed for CFC-11 (41 to 50 year by Volk et al.); updating the CFC-11 lifetime to 52 years (SPARC 2013) would place the CH_4 stratospheric lifetime estimate at 107 years.

There are a number of previous satellite-based measurements of stratospheric methane, beginning with the Stratospheric and Mesospheric Sounder (SAMS) on Nimbus 7 (Jones and Pyle 1984), the Improved Stratospheric and Mesospheric Sounder (ISAMS), the Cryogenic Limb Array Etalon Spectrometer (CLAES), and the Halogen Occultation Experiment (HALOE) on the Upper Atmosphere Research Satellite (UARS) (Remedios et al. 1996; Kumer et al. 1993; Ruth et al. 1997), and more recently from the Atmospheric Chemistry Experiment-Fourier Transform Spectrometer (ACE-FTS) on SCISAT-1 (De Maziere et al. 2008) and the Michelson Interferometer for Passive Atmospheric Sounding (MIPAS) on ENVISAT (Payan et al. 2009; von Clarmann et al. 2009). Although these measurements have proven useful in many science investigations, there is a need for long term, global methane data that spans the entire middle atmosphere—from the tropopause up to the lower mesosphere. The SAMS, ISAMS, and CLAES data records have limited durations of 2 years or less (though in some cases by design), and while the HALOE record covers an impressive length of~13 years, global sampling is limited due to the availability of solar occultations along the UARS orbital path. In particular, HALOE measurements are sparse at high latitudes and there are few measurements above 50°N during NH winter. MIPAS observations ceased in 2012, and the only currently ongoing series of stratospheric methane measurements is from ACE-FTS. This data set has been shown to be useful for examining the structure of the stratospheric polar vortex (e.g., Manney et al. 2009a), as the SCISAT-1 orbital configuration emphasizes observations at high latitudes. However, the solar occultation method of observation limits the number of profiles to ~30 per day, and opportunities for sampling at low latitudes are more limited (~4 months/year) than for high latitudes.

This paper presents a new methane data set derived using coincident measurements of water vapor (H_2O), carbon monoxide (CO), and nitrous oxide (N_2O) from the Microwave Limb Sounder (MLS) instrument on the Aura satellite. Among the advantages of a derived methane product (MLS derived, or MLSD CH_4) are: The altitude range spanned by the use of multiple datasets from MLS allows a derivation of methane vertical distributions from the tropopause up to the lower mesosphere; the nearly global, daily coverage of MLS measurements provides for more than 3000 vertical profiles per day between+−82° latitude; and there are a large number of co-located measurements of reactive and long-lived species (in addition to those used to derive methane), along with measurements of temperature and co-located derived meteorological products (DMPs, Manney et al. 2007), all of which can be used for further analysis.

2 Methods

In addition to methane, there are numerous other long lived tracers (species with local, instantaneous lifetimes greater than quasi-horizontal transport times) in the stratosphere. In

general, the mixing ratio of one tracer plotted against another displays a simple, compact relationship in the extratropical lower stratosphere (Plumb and Ko 1992). In certain circumstances, the presence of horizontal mixing barriers such as those observed between the tropical-extratropical lower stratosphere (e.g., Minschwaner et al. 1996; Plumb 1996), or along the edges of polar winter vortices (e.g., Waugh et al. 1997; Michelsen et al. 1998b; Plumb et al. 2000) can lead to distinctly different populations of tracer-tracer relationships. In the inner tropics and polar vortices, the correlations are also altered by mean upward and mean downward vertical velocities, respectively. While these differences between regimes can be significant, simple and relatively compact relationships may be obtained in a more general sense throughout most of the global stratosphere for species that have similar patterns of stratospheric loss, and whose mean tropospheric mixing ratios do not change rapidly with season or display a large secular rate of increase. The latter condition ensures that entry-level mixing ratios to the stratosphere are not changing appreciably over the mean residence time for air parcels to circulate within the stratosphere (3–7 years, e.g., Engel et al. 2009).

One tracer that is measured by both ACE and MLS is nitrous oxide (N_2O). Figure 1 shows point density contours of a tracer-tracer scatter plot between N_2O and CH_4 from ACE measurements (Bernath et al. 2005; Boone et al. 2005) over the time period 2005–2009. During this time, the global mean tropospheric mixing ratio of N_2O increased from 319 to 323 ppbv, with minimal seasonal variations (Elkins and Dutton 2009). The N_2O increase corresponds to a mean growth rate of 0.24 %/year. At the same time, tropospheric CH_4 mixing ratios increased from a mean of 1775 ppbv to 1800 ppbv (0.28 %/year mean growth rate) with peak-to-peak seasonal changes of ~10 ppbv (Dlugokencky et al. 2015). While these variations are not entirely negligible, their impact on tracer-tracer correlations in stratospheric mixing ratios is small, as seen in the narrow spread in Fig. 1 at the uppermost mixing ratio values.

The tight correlation between CH_4 and N_2O throughout the stratosphere, including the tropics, is a consequence of the similar patterns of stratospheric destruction for these two species. CH_4 is destroyed primarily by reactions with either $O(^1D)$ or OH (Brasseur and Solomon 2005), and the concentration of OH in the stratosphere is governed mainly by production through the reaction $O(^1D) + H_2O \rightarrow 2OH$ (Canty and Minschwaner 2002). Thus, the overall loss rate of CH_4 is set by the availability of $O(^1D)$ which is produced through the ultraviolet photodissociation of O_3. N_2O is destroyed mainly by ultraviolet photodissociation (~90 % of loss) and secondarily by reaction with $O(^1D)$ (Johnston et al. 1979). The destruction rates for both CH_4 and N_2O are dependent on the intensity of solar ultraviolet radiation, but in different wavelength regions (200–220 nm for N_2O versus 280–300 nm for O_3 in the lower stratosphere). However, chemical destruction rates are, in both cases, largest in the low-latitude stratosphere and they both increase monotonically with increasing altitude above the tropopause.

The relationship shown in Fig. 1 is well represented by a polynomial fit that captures the empirical relationship between CH_4 and N_2O. On the basis of the χ^2 goodness of fit, a 4th order polynomial was selected for this representation; the use of higher orders did not significantly reduce χ^2. Coefficients to the fit polynomial are given in Table 1. As this fit spans a 5-year observation period, any interannual variability in the CH_4-N_2O relationship will contribute to the overall uncertainty in MLSD CH_4 mixing ratios. Figure 1 shows the percent differences between fits for individual years of ACE data, compared with the multi-year fit. We find that interannual variations in the fit are less than 2 % for CH_4 mixing ratios greater than 1 ppmv, which corresponds to the lower and middle stratospheric tropical and midlatitude regions. Therefore, the largest contribution to the uncertainty in MLSD methane for mixing ratios greater than about 1 ppmv arises from the spread in ACE CH_4 that is seen at a given value of observed N_2O. This spread is dominated by seasonal and latitudinal variability (see
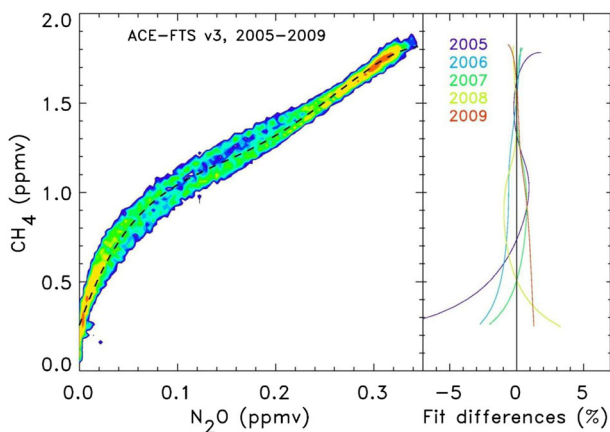
Fig. 1 *Left panel* is a contour plot of the number of measurements obtained at plotted values of N_2O and CH_4 mixing ratios from ACE-FTS data, ranging from *blue* (low density of measurements) to *red* (high density of measurements). The observation period is from 2005 to 2009, for all available latitudes (85°N to 85°S) and between 100 hPa and 0.1 hPa pressure. *Dashed curve* is a 4th degree polynomial fit to sub-sampled data according to filtering criteria discussed in the text. *Right panel* shows differences between fits in individual years compared with the 5-year aggregate fit shown in *left panel*

Electronic Supplement). Differences in the CH_4-N_2O relationship have been noted between tropical and polar vortex observations in the stratosphere (e.g., Michelsen et al. 1998a). As seen in Fig. 1, the spread is small for large values of CH_4 (the extra-polar lower stratosphere) but it increases rapidly for $CH_4 < 1$ ppmv (above the middle stratosphere and in the polar regions). Some of the largest latitudinal differences in tracer-tracer correlations are in the middle and upper stratosphere, and therefore either one (or both) of the following limitations are applied to the fit: either the pressure range of data for the N_2O fit must fall 100 hPa and 30 hPa, or the mixing ratio of N_2O must exceed 0.15 ppmv. The former condition covers the lower strato-sphere at all latitudes, and the latter condition extends this region to include the low-latitude stratosphere up to about 10 hPa. Even with these restrictions, there are small but clear seasonal and latitudinal variations in the N_2O fit, although we did not achieve significant improvements over a single universal fit by using multiple fits to seasonal and latitudinal binned data (see Supplement). Based on the standard deviation of CH_4 versus N_2O, the fit errors from the single fit are about 3 % near 0.34 ppmv N_2O, and increase to 7 % near 0.15 ppmv N_2O.

In the upper stratosphere/lower mesosphere and in the winter polar vortex regions, where methane mixing ratios are less than 1 ppmv, N_2O is no longer a suitable tracer for correlation analysis. However, the correlation between CH_4 and H_2O is well documented in these regions (e.g., Abbas et al. 1996). The oxidation of methane ultimately produces both H_2 and H_2O, although the major fraction of the production leads to water vapor (e.g. Rohs et al. 2006), so that $2CH_4 + H_2O \approx$ constant [Nassar et al. 2005; and references therein]. Figure 2 shows the observed relationship between CH_4 and H_2O from ACE data over the period 2005–2009. These data include bias corrections and latitude/altitude binning that is described in more detail below. For CH_4 mixing ratios between about 0.5 and 1.5 ppmv, we find a nearly linear correlation with a slope of about −0.5. However, there are two regions where this simple relationship breaks down: For $CH_4 > 1.5$ ppmv (mostly in the lower stratosphere) there is a large spread in H_2O that most likely results from stratosphere-troposphere exchange and variability in factors controlling the water vapor inputs to the stratosphere, such as the seasonal variation in tropical tropopause temperatures. Thus, a flattening of the correlation contours is

Table 1 Coefficients of polynomial functions for CH_4 derived from simultaneous measurements of N_2O, H_2O, and CO. ($y=A+Bx+Cx^2+Dx^3+Ex^4$, where y and x are in units of ppmv)

Coefficient	$y=CH_4$, $x=N_2O$ valid for $100<p<30$ hPa or $N_2O>0.15$ ppmv	$y=CH_4$, $x=H_2O$ valid for $p<30$ hPa and $N_2O<0.15$ ppmv and $CO<0.14$ ppmv	$y=CH_4$, $x=H_2O$ valid for $p<30$ hPa and $N_2O<0.15$ ppmv and $CO>0.14$ ppmv
A	0.2109	−4.636	0.1414
B	11.44	4.965	−0.1076
C	−57.91	−1.312	2.920×10^{-2}
D	177.5	0.1339	-1.827×10^{-3}
E	−190.0	-4.751×10^{-3}	

observed near the top of Fig. 2. As discussed above, we use N_2O to derive CH_4 in this region, so the correlation breakdown here has no impact on our analysis.

For $CH_4<0.5$ ppmv (mostly the mesosphere), the linear relationship in Fig. 2 reverses direction, and both CH_4 and H_2O monotonically decrease to zero values. Mixing ratios of H_2 correspondingly increase at higher altitudes, and H_2 becomes a significant component of the hydrogen budget in the mesosphere (Engel et al. 2006). The reversal in the CH_4-H_2O correlation is a result of photochemical destruction of both CH_4 and H_2O, with the latter occurring from ultraviolet photolysis at Lyman-alpha and Schumann-Runge band wavelengths (Nicolet 1984). This correlation regime is also observed for air parcels within the winter polar vortices since these parcels have generally descended from higher altitudes (e.g., Fisher et al. 1993; Manney et al. 1994). A reliable indicator of air that is near or above the stratopause, or of air that originated at such high altitudes, is the mixing ratio of carbon monoxide (CO) (e.g., Allen et al. 1999). The CO mixing ratio is generally small throughout most of the stratosphere due to its destruction by reaction with OH, but above the stratopause there is an increasing source from the photodissociation of CO_2, leading to increasing mixing ratios with altitude and high CO levels within the winter polar vortex due to descent (e.g., Minschwaner et al. 2010).
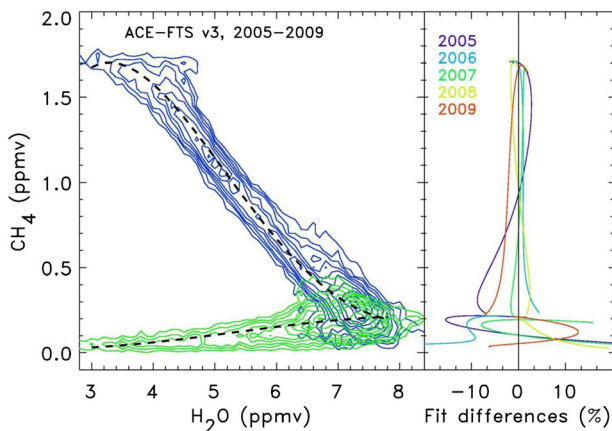
Fig. 2 Same as Fig. 1, except for H_2O and CH_4 from ACE-FTS measurements. Unfilled contours in *left panel* are color coded according to coincident measurements of CO, with blue contours for $CO<0.14$ ppmv and *green* contours for $CO>0.14$ ppmv. The ACE data have been scaled to match MLS measurements, and have been binned within a fixed latitude/altitude grid as described in the text

We use ACE measurements of CO to distinguish between the two CH_4-H_2O correlation regimes from ACE shown in Fig. 2, and apply a CO threshold of 0.14 ppmv for this purpose. Table 1 lists the coefficients for a 4th order polynomial fit to the CH_4-H_2O correlation in the middle and upper stratosphere (CO<0.14 ppmv), and coefficients for a 3rd order polynomial for the mesosphere and polar vortex regions (CO>0.14 ppmv). As indicated in Fig. 2, interannual variability plays a much larger role in the overall uncertainty of methane derived using this technique than for that derived using the N_2O relationship, and can be as large as 15 %. The overall uncertainty, however, is still dominated by the scatter in CH_4 for given CO and H_2O values; it ranges from 12 % near 1.0 ppmv CH_4, to 30 % at 0.2 ppm CH_4 (near the regime cross-over), increasing to 60 % at 0.05 ppmv CH_4. Seasonal and latitudinal variations in CH_4-H_2O correlations do play a role in the observed spread of CH_4 values (see Electronic Supplement), but only for relatively higher values of CH_4 where the fit uncertainty is small; at very low CH_4 mixing ratios, the spread is more dominated by measurement precision than by geophysical variability. We therefore adopt this universal combination of fits rather than applying multiple fits for individual seasons and latitude ranges.

MSLD CH_4 mixing ratios are produced on nineteen pressure levels (six per decade in log p) between 100 hPa and 0.1 hPa at all latitudes, longitudes, and times where there are useful MLS measurements of N_2O in the lower stratosphere, or simultaneous measurements of H_2O and CO at higher altitudes. Data screening is applied according to recommendations for each species outlined in the MLS v3.3 Data Quality and Description Document (Livesey et al. 2011).

There are two important adjustments that have been applied to the ACE data shown in Figs. 1 and 2 in order to transfer the foregoing results to MLS data for deriving methane mixing ratios. The first relates to latitude- and altitude-dependent offsets between ACE and MLS zonal mean mixing ratios of N_2O, H_2O, and CO. The functional relationships used for MLSD CH_4 are based entirely on observed ACE tracer correlations so that any offsets between ACE and MLS measurement of these tracers will propagate through, in a nonlinear fashion, to the derived methane. In order to reduce this effect, zonal and seasonal mean differences between ACE and MLS N_2O, H_2O, and CO were computed and used to scale all ACE measurements of these tracers to better agree with MLS data. Relative magnitudes of the differences typically range between ±20 %. Most of these biases have been explored in previous validation papers (Pumphrey et al. 2007; Lambert et al. 2007) and are not the focus of this paper; they will not be presented in detail. Note that the adjustments applied here are not based on any judgments concerning the relative accuracy of either dataset, but rather they are necessary in order for the MLSD CH_4 to be consistent with the CH_4 measured by ACE.

A second adjustment to the ACE datasets was necessary in order to reduce the impact of non-uniform latitude and seasonal sampling. The nature of the SCISAT platform orbit, in combination with the occultation measurement technique of ACE, favors mid/high latitude sampling (~30° to 70°) over the lower latitudes. Latitude sampling would not be an issue if the tracer-tracer correlations were truly global, but for certain ranges of N_2O or H_2O mixing ratios, the resulting correlation with CH_4 is clearly latitude dependent. For example, Fig. 3 shows ACE H_2O and CH_4 data from 2005 binned from two latitude regions, ±10° and 60–65°N. This scatterplot demonstrates that the low-latitude data generally have larger CH_4 mixing ratios for a given value of H_2O in the middle and upper stratospheric regions, particularly for H_2O near 7 ppmv. As a result, a fit based on the raw data would be shifted toward smaller CH_4 mixing ratios characteristic of high latitudes where the ACE sampling frequency is much higher. Such fits will produce a significant low bias in derived CH_4 at lower latitudes. In order to obtain more general global relationships between tracers, we bin-averaged the raw ACE data within uniform altitude and latitude grids prior to generating fits to the scatterplots.
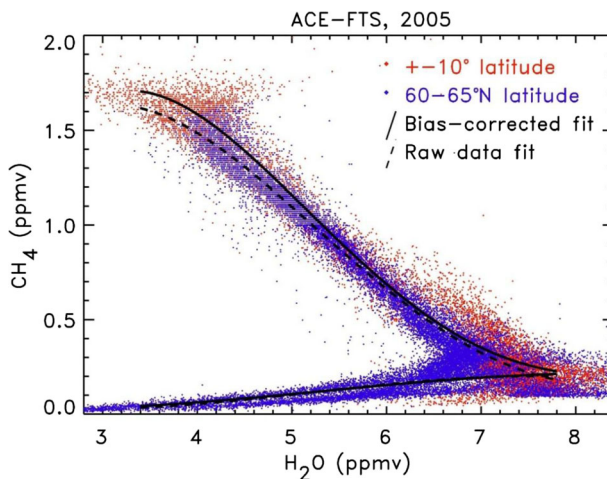
Fig. 3 Scatter plot of CH_4 versus H_2O from 2005 ACE-FTS measurements within +−10° latitude (*red* data points), and within 60–65°N latitude (*blue* data points), along with the sampling bias-corrected fit to the 2005 data (*solid curves*), and the uncorrected, raw fit all 2005 data (*dashed curve*)

3 Results

A previous version of derived methane (Minschwaner et al. 2010) was compared with ACE and HALOE measurements in limited cases where close spatial and temporal measurement coincidences were found. Agreement was within +−20 % in the middle stratosphere, although larger discrepancies were present at higher altitudes; this earlier version also did not extend into the lower stratosphere, and did not account for latitude sampling biases in the tracer-tracer correlations.

We show monthly zonal means here in order to compare a wider range of times, latitudes, and altitudes. Figure 4 shows comparisons for two pressure levels (4.64 and 0.464 hPa) and two latitude ranges (0–10°N and 50–60°N). At the lower latitudes, agreement with both HALOE and ACE is very good at both pressure levels. At 4.64 hPa mean differences are on the order of 10 % and the seasonal and interannual variability is well matched. At 0.46 hPa the mean differences are larger (20 %) and, although the seasonal phase agrees with that in ACE measurements, the amplitude of the seasonal cycle in MLSD CH_4 is about three times smaller than that in the ACE data. Inspection of the HALOE data in this case suggests that the seasonal amplitude may lie between that of MLSD and ACE, although the overlap in the time series is too short for a definitive comparison. At high latitudes, MLSD appears to be biased high by ~15 % at 4.64 hPa, and 30–60 % at 0.46 hPa, with respect to ACE. The amplitude and phase of the seasonal cycle appear to agree reasonably well between MLSD and ACE CH_4 at 4.64 hPa, whereas at 0.46 hPa the phase is clearly shifted by 4–6 months. The shorter HALOE record does not clearly indicate which dataset displays a more reliable seasonal cycle at this pressure and latitude. In the case of either HALOE or ACE data, it should be noted that sampling limitations restrict the availability of zonal means for every month, and even in months where zonal means can be computed, the number of measurements used for HALOE or ACE means is significantly less than the number used for MLSD monthly means (on the order of 10–50 profiles for HALOE and ACE in 10° latitude bins, compared to ~5,000 profiles for MLSD).

To examine a larger range of pressures and latitudes, we compare MLSD and ACE zonal, annual means for 2010 in Fig. 5. Throughout most of the global stratosphere, agreement is
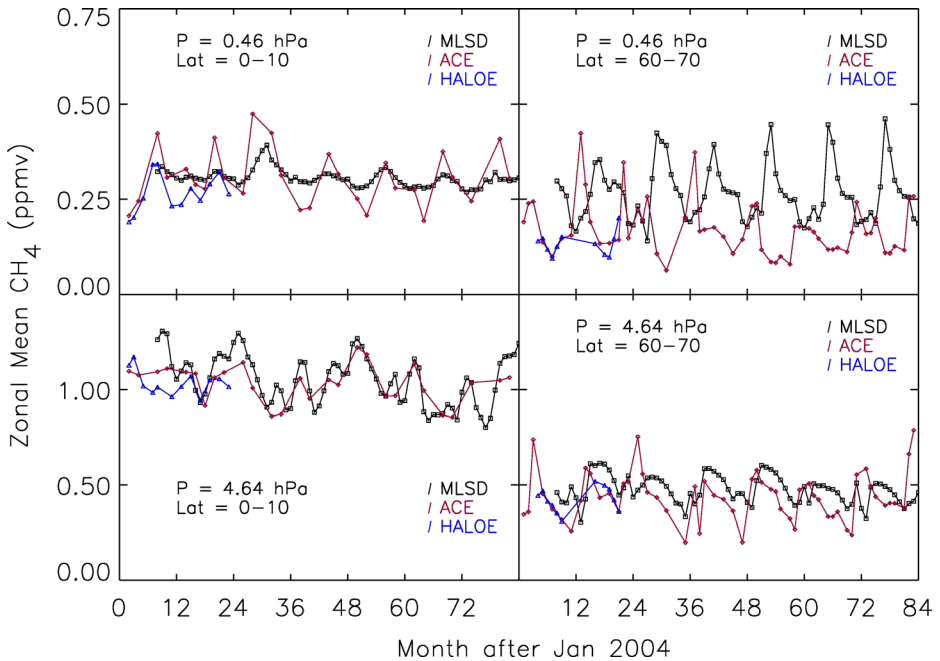
Fig. 4 Time series of zonally averaged, monthly mean CH$_4$ at 0.464 hPa (*top*) and 4.64 hPa (*bottom*) for the latitude ranges 0–10°N (*left*) and 50–60°N (*right*). Plotted data are the MLSD (*black*), ACE-FTS (*red*), and HALOE (*blue*)

quite good and differences are less than 15 %. The largest differences generally occur in the low latitude, middle to upper stratosphere where MLSD methane is about 20–40 % lower than ACE methane. Another area of larger differences occurs in the high latitude upper stratosphere/ lower mesosphere, where MLSD can be up to 20–40 % higher than ACE. Methane mixing ratios are very low here, however, and absolute differences are actually only 0.1–0.2 ppmv. The general pattern of differences seen in Fig. 5 is consistent between different seasons and years, and thus reflects systematic offsets from multiple sources, including the fitting algorithm, residual bias from non-uniform latitude sampling, and remaining biases between ACE
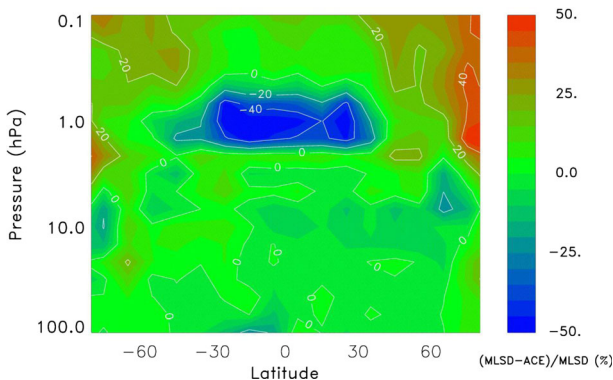
Fig. 5 Contours of percent differences between zonal and monthly mean MLSD and ACE CH$_4$, averaged over the year 2010. These differences have been computed using zonal monthly mean differences averaged over all months of the year

and MLS N_2O, H_2O, and CO that are not removed by the differencing scheme discussed above. It is also important to note that combined uncertainties in the MLS N_2O, H_2O, and CO used to generate derived methane cannot be neglected, even in zonal means.

One application of MLSD CH_4 fields is as a tracer for examining the structure and evolution of the wintertime polar vortex. The near global daily coverage of MLS observations makes its N_2O and CO measurements valuable for studying transport in polar winter, especially descent in the vortex (e.g., Manney et al. 2008b, 2009a, b; Lee et al. 2011; McDonald and Smith 2013). N_2O and CO, however, provide only separate views of the lower stratosphere or upper stratosphere/lower mesosphere, respectively. Using MLSD CH_4 vortex averages, we can investigate the stratospheric and lower-mesospheric vortex as a whole. Figure 6 shows vortex averages on isentropic surfaces during the 2005–06 Northern Hemisphere winter season. MSLD vortex averages are shown along with corresponding means of simulated CH_4 fields from the SLIMCAT model and from CMAM-DAS (Canadian Middle Atmosphere Model—Data Assimilation System). SLIMCAT is a 3-D chemical transport
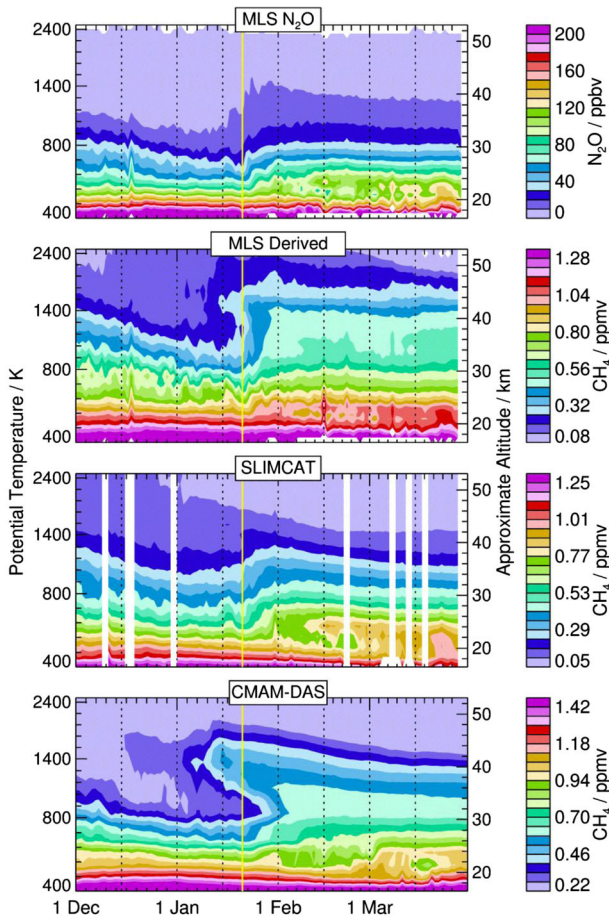
Fig. 6 Time evolution of vortex averaged (within 1.4×10^{-4} s^{-1} sPV contour) N_2O (*top panel*) and CH_4 versus potential temperature for the Northern Hemisphere 2005–2006 winter season. MLSD (*second panel*), SLIMCAT model driven by ECMWF winds and temperatures (*third panel*), and CMAM-DAS with assimilated transport dynamics (*bottom panel*)

model driven by winds and temperatures from ECMWF analyses (Chipperfield 1999, 2006). The SLIMCAT simulations are from a parallel run that was sampled at the MLS measurement times and locations, described in more detail in Manney et al. 2009a. The CMAM-DAS results are from the online transport code included in the CMAM atmospheric general circulation model with interactive chemistry and radiation (de Grandpre et al. 2000; Scinocca et al. 2008), coupled with a data assimilation system that incorporates wind and temperature observations using the 3D-VAR assimilation scheme (Polavarapu et al. 2005; Ren et al. 2011).

Comparison of the vortex averages in Fig. 6 shows similarities in the patterns of descent within the polar vortex, as CH_4 isopleths gradually descend in the lower stratosphere at rates of ~1.5 km/month from December to mid-January. The observations and simulations clearly show the impact of the major stratospheric sudden warming (SSW) that began in late January 2006 (e.g., Manney et al. 2008a, 2009a; and references therein). Studies of this major SSW showed a complete breakdown of the polar vortex throughout the middle and upper strato-sphere, followed by reformation of an unusually strong vortex in the upper stratosphere/lower mesosphere, and enhanced descent into that reformed vortex (e.g., Manney et al. 2008a, b, 2009a; Randall et al. 2006). Figure 6 shows the effects of the SSW, with abrupt increases in vortex-averaged CH_4 during the event, as higher mixing ratios of CH_4 from lower latitudes are mixed into the remnants of the polar vortex. Both MLSD and CMAM-DAS indicate a "top-down" breakdown of the vortex, with CH_4 showing the effects of mixing earlier at higher than at lower altitudes. The SLIMCAT results do not reflect this behavior, although it appears from the overall evolution of the SLIMCAT averages that this simulation reflects larger rates of mixing across the vortex edge than seen in either MLSD or CMAM-DAS. As shown by Manney et al. (2008a), the ECMWF data assimilation system does very poorly at representing the meteorology of the upper stratosphere/lower mesospheric during this extreme event, especially with regard to descent rates. These failings are responsible for some of the deficiencies seen in the ECMWF representation of transport during this event. Comparing the absolute values of CH_4 vortex averages, SLIMCAT and MLSD are in good agreement, while CMAM-DAS consistently displays higher values with an offset of about 0.1–0.2 ppmv. This likely results at least partly from the fact that MLS values of N_2O (as well as O_3, HNO_3, HCl, H_2O, and smoothed and zonally averaged values of CO) were used in the initialization of the SLIMCAT run [Manney et al. 2009a], whereas the CMAM-DAS run was initialized with a climatology. As can be seen in the top panel of Fig. 6, the variations in the middle to upper stratosphere cannot be seen in N_2O, while the expected good agreement is seen in the lower stratosphere.

Figure 7 shows a comparison of the time evolution of daily mean fields as a function of equivalent latitude (the latitude that would enclose the same area between it and the pole as a given potential vorticity contour [Butchart and Remsberg 1986], useful as a polar-vortex centered coordinate) for MLSD CH_4, and MLS H_2O, N_2O, and CO. Data are binned and averaged in equivalent latitude and time on the 850 K potential temperature surface (near 10 hPa pressure, or 30 km altitude). At this level, MLSD CH_4 is derived primarily from N_2O at low latitudes, and from H_2O at mid-to-high latitudes. The patterns seen in both CH_4 and N_2O are thus quite similar equatorward of 20° latitude. As discussed in Section 2, the transition between a derivation based on N_2O and one based on H_2O is dictated by the amount of N_2O (>0.15 ppmv). Where MLSD CH_4 is derived from H_2O, we apply two very different correlations, with the transition dictated by the corresponding level of CO (0.14 ppmv threshold). Figure 7 shows very low values of CO at low and middle latitudes, and the use of a single CH_4-H_2O relationship is suitable here. As this is an inverse relationship for low CO (Section 2), the patterns seen in CH_4 and H_2O are similar but opposite in sign. Within the late-winter and springtime vortices, however, elevated levels of CO indicate exposure to high-

altitude photochemical conditions that require the alternative, positive CH_4-H_2O correlation discussed in Section 2. Large CO gradients that separate the inner vortex from the outer edges (denoted by the black PV contours in Fig. 7) are extremely useful for mapping CH_4 to the appropriate correlation with H_2O in these regions. The good correspondence seen between MLSD CH_4 fields and the other tracers indicates the derivation algorithm works well across all seasons and years.

The results shown in Fig. 7 also demonstrate that at the 850 K level, N_2O provides useful tracer fields for examining transport at low and middle latitudes, but rapidly decreasing mixing ratios within the polar vortices reduce the information content at high latitudes in winter and spring. Conversely, CO mixing ratios are high enough to be useful for diagnosing transport only within the inner vortex during late winter and spring. H_2O fields span a comparatively larger useful latitude range, but gradients in the deep tropics are weaker than for N_2O, and the mid-to-high latitude patterns are more complex due to the morphology of H_2O. CH_4 fields are thus the option that provides information on transport over the widest possible range of latitudes and meteorological regimes, and we will focus attention on CH_4 for the remaining discussion of Fig. 7.

In the deep tropics, there is an annual CH_4 cycle near the equator with largest mixing ratios during March-April. This cycle is clearly modulated by the quasi-biennial oscillation in zonal winds (QBO, shown at the top of Fig. 7), with peak mixing ratios occurring only during the easterly QBO phase at 10 hPa. During westerly phases, the springtime equatorial CH_4 maximum is significantly suppressed.
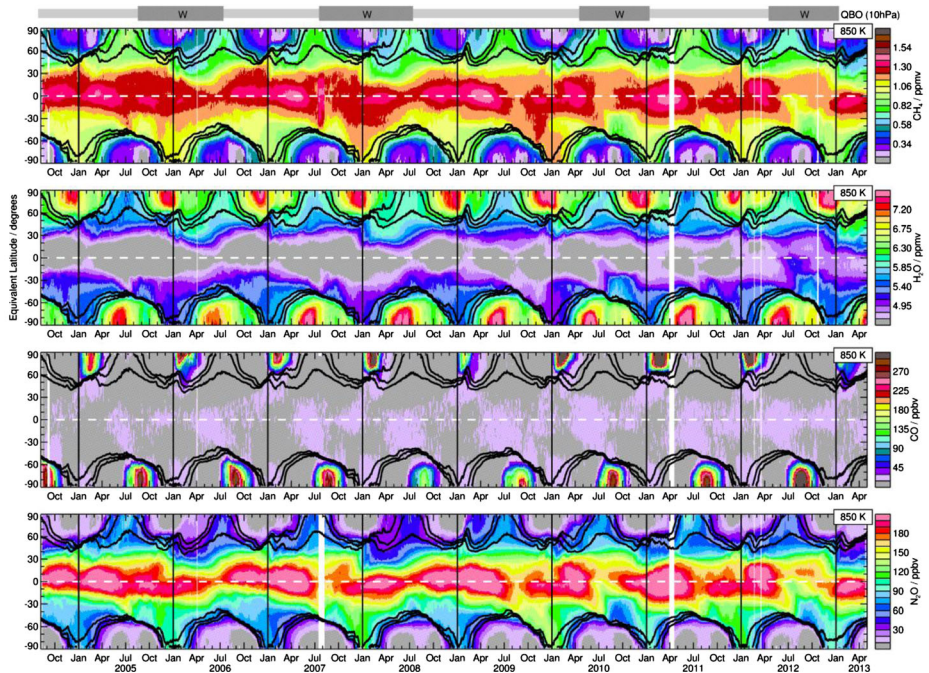
Fig. 7 Time series plots of daily mean CH_4, H_2O, CO, and N_2O mixing ratios on the 850 K potential temperature surface, gridded in equivalent latitude and time as described by *Manney* et al. [2007]. N_2O, H_2O, and CO values are from MLS measurements; CH_4 values are from the MLSD fields. Overlays are contours of scaled PV demarking the polar vortex edge region. Grey bars at top give the phase of the QBO determined by the direction of Singapore winds at 10 hPa

Large CH_4 gradients at the sub-tropical boundary separating the tropics from midlatitudes demonstrate the isolation of the tropical "pipe" region [e.g., Plumb 1996; Minschwaner et al. 1996]. Enhanced transport from the subtropics to high latitudes is observed during summer, and this transport appears to be more efficient in the Southern Hemisphere (SH). Higher mixing ratios appear to reach the SH pole in January than in the Northern Hemispheric (NH) pole in July. Signatures of decent in, and isolation of, the winter polar vortices are evident from the CH_4 fields, and there are also clear signs of mixing into the polar vortex region during strong NH SSWs, particularly in early 2006 and 2009. The unusually strong and long-lasting NH vortex in 2011 is evident from the low CH_4 mixing ratios that persisted well into the late spring of 2011.

4 Conclusions

We have described a new methane data set for middle atmospheric composition and transport studies. Techniques for deriving methane were developed using coincident measurements of N_2O, H_2O, and CO from the ACE-FTS satellite instrument, and the derivation algorithm was implemented using MLS measurements of these trace gases. The methodology includes scaling adjustments to account for offsets between ACE-FTS and MLS observed tracer fields, and uniform latitude weighting in the correlation analysis of ACE-FTS data to reduce the impact of latitude sampling biases.

MLS measurements of N_2O are used to derive the new methane data product in the lower stratosphere, while MLS measurements of H_2O are used to derive CH_4 in the upper stratosphere and lower mesosphere. Coincident MLS measurements of CO are used to distinguish between two distinct chemical regimes observed in the CH_4—H_2O correlation from ACE-FTS. Methane mixing ratios are produced on nineteen pressure levels between 100 hPa and 0.1 hPa, with full coverage over latitude (up to 82°), longitude, and seasons, from 2004 to 2013. The derived CH_4 fields agree with ACE-FTS measurements to within ±15 % on average, although some differences can be as large as 40 % within isolated regions of the middle atmosphere.

The derived methane fields have the potential to expand understanding of dynamical processes affecting middle atmospheric composition, such as upwelling in the tropical lower stratosphere and the influence of the quasi-biennial oscillation, mean transport by the Brewer-Dobson circulation, and descent in the wintertime polar vortices and the impact of stratospheric sudden warmings. The effects of other transport processes that can be observed in this data set include quasi-isentropic mixing between the tropics and extratropics, and mixing across transport barriers such as the polar vortex edge. For all of these processes, comparison of the derived methane fields to model outputs, either in free-running dynamical mode or driven by assimilated winds, provides a useful test of the representation of trace gas transport in model simulations. The full data set with standard daily l2gp files in hdf5 format can be obtained upon email request from the lead author, or online from http://mls.jpl.nasa.gov/data/ch4.php.

References

Abbas, M.M., Gunson, M.R., Newchurch, M.J., Michelsen, H.A., Salawitch, R.J., Allen, M., Abrams, M.C., Chang, A.Y., Goldman, A., Irion, F.W., Moyer, E.J., Nagaraju, R., Rinsland, C.P., Stiller, G.P., Zander, R.: The hydrogen budget of the stratosphere inferred from ATMOS measurements of H_2O and CH_4. Geophys Res Lett **23**, 2405–2408 (1996)

Allen, D.R., Stanford, J.L., Lopez-Valverde, M.A., Nakamura, N., Lary, D.J., Douglass, A.R., Cerniglia, M.C., Remedios, J.J., Taylor, F.W.: Observations of middle atmosphere CO from the UARS ISAMS during the early northern winter 1991/1992. J Atmos Sci **56**, 563–583 (1999)

Bernath, P.F., McElroy, C.T., Abrams, M.C., Boone, C.D., Butler, M., Camy-Peyret, C., Carleer, M., Clerbaux, C., Coheur, P.F., Colin, R., DeCola, P., DeMaziere, M., Drummond, J.R., Dufour, D., Evans, W.F.J., Fast, H., Fussen, D., Gilbert, K., Jennings, D.E., Llewellyn, E.J., Lowe, R.P., Mahieu, E., McConnell, J.C., McHugh, M., McLeod, S.D., Michaud, R., Midwinter, C., Nassar, R., Nichitiu, F., Nowlan, C., Rinsland, C.P., Rochon, Y.J., Rowlands, N., Semeniuk, K., Simon, P., Skelton, R., Sloan, J.J., Soucy, M.A., Strong, K., Tremblay, P., Turnbull, D., Walker, K.A., Walkty, I., Wardle, D.A., Wehrle, V., Zander, R., Zou, J.: Atmospheric Chemistry Experiment (ACE): mission overview. Geophys Res Lett **32**, L15S01 (2005). doi:10.1029/2005GL022386

Boone, C.D., Nassar, R., Walker, K.A., Rochon, Y., McLeod, S.D., Rinsland, C.P., Bernath, P.F.: Retrievals for the atmospheric chemistry experiment Fourier-transform spectrometer. Appl Opt **44**, 7218–7231 (2005)

Brasseur, G., Solomon, S.: Aeronomy of the middle atmosphere, 3rd edn. Springer, Dordrecht (2005)

Butchart, N., Remsberg, E.E.: The area of the stratospheric polar vortex as a diagnostic for tracer transport on an isentropic surface. J Atmos Sci **43**, 1319–1339 (1986)

Canty, T., Minschwaner, K.: Seasonal and solar cycle variability of OH in the middle atmosphere. J Geophys Res **107**, 4737 (2002). doi:10.1029/2002JD002278

Chipperfield, M.P.: Multiannual simulations with a three dimensional chemical transport model. J Geophys Res **104**, 1781–1805 (1999)

Chipperfield, M.P.: New version of the TOMCAT/SLIMCAT offline chemical transport model: intercomparison of stratospheric tracer experiments. Q J R Meteorol Soc **132**, 1179–1203 (2006)

de Grandpre, J., Beagley, S.R., Fomichev, V.I., Griffioen, E., McConnell, J.C., Medvedev, A.S.: Ozone climatology using interactive chemistry: results from the Canadian middle atmosphere model. J Geophys Res **105**, 26,475–26,491 (2000)

De Maziere, M., et al.: Validation of ACE-FTS v2.2 methane profiles from the upper troposphere to the lower mesosphere. Atmos Chem Phys **8**, 2421–2435 (2008)

Dlugokencky, E.J., P.M. Lang, A.M. Crotwell, and K.A. Masarie, Atmospheric Methane Dry Air Mole Fractions from the NOAA ESRL Carbon Cycle Cooperative Global Air Sampling Network, 1983–2013, Version: 2014-06-24, Path: ftp://ftp.cmdl.noaa.gov/ccg/ch4/flask/event/ (2014)

Elkins, J.W., Dutton, G.S.: Nitrous oxide and sulfur hexafluoride [in 'State of the climate in 2008']. Bull Am Meteorol Soc **90**, S38–S39 (2009)

Engel, A., Mobius, T., Haase, H.P., Bonisch, H., Wetter, T., Schmidt, U., Levin, I., Reddmann, I.T., Oelhaf, H., Wetzel, G., Grunow, K., Huret, N., Pirre, M.: Observation of mesospheric air inside the arctic stratospheric polar vortex in early 2003. Atmos Chem Phys **6**, 267–282 (2006)

Engel, A., Mobius, T., Bonisch, H., Schmidt, U., Heinz, R., Levin, I., Aoki, S., Nakazawa, T., Sugawara, S., Moore, F., Hurst, D., Elkins, J., Schauffler, S., Andrews, A., Boering, K.: Age of stratospheric air unchanged within uncertainties over the past 30 years. Nat Geosci **2**, 28–31 (2009). doi:10.1038/Ngeo388

Fisher, M., O'Neill, A., Sutton, R.: Rapid descent of mesospheric air into the stratospheric polar vortex. Geophys Res Lett **20**, 1267–1270 (1993)

Johnston, H.S., Serang, O., Podolske, J.: Instantaneous global nitrous oxide photochemical loss rates. J Geophys Res **84**, 5077–5082 (1979)

Jones, R.L., Pyle, J.A.: Observations of CH4 and N2O by the Nimbus7 SAMS—a comparison with in situ data and two-dimensional numerical-model calculations. J Geophys Res **89**, 5263–5279 (1984)

Kumer, J.B., Mergenthaler, J.L., Roche, A.E.: CLAES CH_4, N_2O, and CCl_2F_2 (F12) global data. Geophys Res Lett **20**, 1239–1242 (1993)

Lambert, A., et al.: Validation of the Aura Microwave Limb Sounder middle atmosphere water vapor and nitrous oxide measurements. J Geophys Res **112**, D24S36 (2007). doi:10.1029/2007JD008724

Lee, J.N., Wu, D.L., Manney, G.L., Schwartz, M.J., Lambert, A., Livesey, N.J., Minschwaner, K., Pumphrey, H.C., Read, W.G.: Aura Microwave Limb Sounder observations of the polar middle atmosphere: dynamics and transport of CO and H_2O. J Geophys Res **115**, D05110 (2011). doi:10.1029/2010JD014608

Livesey, N. J., et al., Aura Microwave Limb Sounder (MLS) Version 3.3 Level 2 Data Quality and Description Document, JPL D-33509 (2011)

Manney, G.L., Zurek, R.W., O'Neill, A., Swinbank, R.: On the motion of air through the stratospheric polar vortex. J Atmos Sci **51**, 2973–2994 (1994)

Manney, G.L., et al.: Solar occultation satellite data and derived meteorological products: sampling issues and Comparisons with Aura MLS. J Geophys Res **112**, D24S50 (2007). doi:10.1029/2007JD008709

Manney, G.L., et al.: The evolution of the stratopause during the 2006 major warming: satellite data and assimilated meteorological analyses. J Geophys Res **113**, D11115 (2008a). doi:10.1029/2007JD009097

Manney, G.L., Daffer, W.H., Strawbridge, K.B., Walker, K.A., Boone, C.D., Bernath, P.F., Kerzenmacher, T., Schwartz, M.J., Strong, K., Sica, R.J., Krüger, K., Pumphrey, H.C., Lambert, A., Santee, M.L., Livesey, N.J., Remsberg, E.E., Mlynczak, M.G., Russell III, J.R.: The high Arctic in extreme winters: vortex, temperature, and MLS and ACE-FTS trace gas evolution. Atmos Chem Phys **8**, 505–522 (2008b)

Manney, G.L., Harwood, R.S., MacKenzie, I.A., Minschwaner, K., Allen, D.R., Santee, M.L., Walker, K.A., Hegglin, M.I., Lambert, A., Pumphrey, H.C., Bernath, P.F., Boone, C.D., Schwartz, M.J., Livesey, N.J., Daffer, W.H., Fuller, R.A.: Satellite observations and modelling of transport in the upper troposphere through the lower mesosphere during the 2006 major stratospheric sudden warming. Atmos Chem Phys **9**, 4775–4795 (2009a)

Manney, G.L., Schwartz, M.J., Kruger, K., Santee, M.L., Pawson, S., Lee, J.N., Daffer, W.H., Fuller, R.A., Livesey, N.J.: Aura Microwave Limb Sounder observations of dynamics and transport during the record-breaking 2009 Arctic stratospheric major warming. Geophys Res Lett **36**, L12815 (2009b). doi:10.1029/2009GL038586

McDonald, A.J., Smith, M.: A technique to identify vortex air using carbon monoxide observations. J Geophys Res **118**, 12719–12733 (2013). doi:10.1002/2012JD019257

Michelsen, H.A., Manney, G.L., Gunson, M.R., Rinsland, C.P., Zander, R.: Correlations of stratospheric abundances of CH_4 and N_2O derived from ATMOS measurements. Geophys Res Lett **25**, 2777–2780 (1998a)

Michelsen, H.A., Manney, G.L., Gunson, M.R., Zander, R.: Correlations of stratospheric abundances of NO_y, O_3, N_2O, and CH_4 derived from ATMOS measurements. J Geophys Res **103**(D21), 28,347–28,359 (1998b)

Minschwaner, K., Dessler, A.E., Elkins, J.W., Volk, C.M., Fahey, D.W., Loewenstein, M., Podolske, J.R., Roche, A.E., Chan, K.R.: Bulk properties of isentropic mixing into the tropics in the lower stratosphere. J Geophys Res **101**, 9433–9439 (1996)

Minschwaner, K., Manney, G.L., Livesey, N.J., Pumphrey, H.C., Pickett, H.M., Froidevaux, L., Lambert, A., Schwartz, M.J., Bernath, P.F., Walker, K.A., Boone, C.D.: The photochemistry of carbon monoxide in the stratosphere and mesosphere evaluated from observations by the microwave limb sounder on the aura satellite. J Geophys Res **115**, D13303 (2010). doi:10.1029/2009JD012654

Myhre, G., Shindell, D., Bréon, F.-M., Collins, W., Fuglestvedt, J., Huang, J., Koch, D., Lamarque, J.-F., Lee, D., Mendoza, B., Nakajima, T., Robock, A., Stephens, G., Takemura, T., Zhang, H.: Climate change 2013: the physical science basis. Contribution of Working Group I to the fifth assessment report of the intergovernmental panel on climate change. In: Stocker, T.F., Qin, D., Plattner, G.-K., Tignor, M., Allen, S.K., Boschung, J., Nauels, A., Xia, Y., Bex, V., Midgley, P.M. (eds.) Anthropogenic and natural radiative forcing. Cambridge University Press, Cambridge (2013)

Nassar, R., Bernath, P.F., Boone, C.D., Manney, G.L., McLeod, S.D., Rinsland, C.P., Skelton, R., Walker, K.A.: Stratospheric abundances of water and methane based on ACE-FTS measurements. Geophys Res Lett **32**, L15S04 (2005). doi:10.1029/2005GL022383

Nicolet, M.: On the photodissociation of water vapour in the mesosphere. Planet Space Sci **32**, 871–880 (1984)

Payan, S., et al.: Validation of version-4.61 methane and nitrous oxide observed by MIPAS. Atmos Chem Phys **9**, 413–442 (2009)

Plumb, R.A.: A "tropical pipe" model of stratospheric transport. J Geophys Res **101**, 3957–3972 (1996)

Plumb, R.A., Ko, M.K.W.: Interrelationships between mixing ratios of long-lived stratospheric constituents. J Geophys Res **97**, 10145–10156 (1992)

Plumb, R.A., Waugh, D.W., Chipperfield, M.P.: The effects of mixing on tracer relationships in the polar vortices. J Geophys Res **105**, 10,047–10,062 (2000)

Polavarapu, S., Ren, S., Rochon, Y., Sankey, D., Ek, N., Koshyk, J., Tarasick, D.: Data assimilation with the Canadian Middle Atmosphere Model. Atmosphere-Ocean **43**, 77–100 (2005)

Pumphrey, H.C., et al.: Validation of middle-atmosphere carbon monoxide retrievals from the Microwave Limb Sounder on Aura. J Geophys Res **112**, D24S38 (2007). doi:10.1029/2007JD008723

Randall, C.E., Harvey, V.L., Singleton, C.S., Bernath, P.F., Boone, C.D., Kozyra, J.U.: Enhanced NOx in 2006 linked to strong upper stratospheric Arctic vortex. Geophys Res Lett **33**, L18811 (2006). doi:10.1029/2006GL027160

Remedios, J.J., Ruth, S.L., Rodgers, C.D., Taylor, F.W., Roche, A.E., Gille, J.C., Gunson, M.R., Russell, J.M., Park, J., Zipf, E.C., Erdman, P.W.: Measurements of methane and nitrous oxide distributions by the

improved stratospheric and mesospheric sounder: retrieval and validation. J Geophys Res **101**, 9843–9871 (1996). doi:10.1029/95JD02840

Ren, S., Polavarapu, S., Beagley, S.R., Nezlin, Y., Rochon, Y.J.: The impact of gravity wave drag on mesospheric analyses of the 2006 stratospheric major warming. J Geophys Res **116**, D19116 (2011). doi:10.1029/2011JD015943

Rohs, S., Schiller, C., Riese, M., Engel, A., Schmidt, U., Wetter, T., Levin, I., Nakazawa, T., Aoki, S.: Long-term changes of methane and hydrogen in the stratosphere in the period 1978–2003 and their impact on the abundance of stratospheric water vapor. J Geophys Res **111**, D14315 (2006). doi:10.1029/2005JD006877

Ruth, S., Kennaugh, R., Gray, L.J., Russell III, J.M.: Seasonal, semiannual, and interannual variability seen in measurements of methane made by UARS Halogen Occultation Experiment. J Geophys Res **102**, 16,189–16,199 (1997)

Scinocca, J.F., McFarlane, N.A., Lazare, M., Li, J., Plummer, D.: The CCCma third generation AGCM and its extension into the middle atmosphere. Atmos Chem Phys **8**, 7055–7074 (2008). doi:10.5194/acp-8-7055-2008

Solomon, S., Rosenlof, K.H., Portmann, R.W., Daniel, J.S., Davis, S.M., Sanford, T.J., Plattner, G.K.: Contributions of stratospheric water vapor to decadal changes in the rate of global warming. Science **327**, 1219–1223 (2010)

SPARC Report on the Lifetimes of Stratospheric Ozone-Depleting Substances, Their Replacements, and Related Species, M. Ko, P. Newman, S. Reimann, S. Strahan (Eds.), SPARC Report No. 6, WCRP-15/2013

Volk, C.M., Elkins, J.W., Fahey, D.W., Dutton, G.S., Gilligan, J.M., Loewenstein, M., Podolske, J.R., Chan, K.R., Gunson, M.R.: Evaluation of source gas lifetimes from stratospheric observations. J Geophys Res **102**, 25543–25564 (1997)

von Clarmann, T., Höpfner, M., Kellmann, S., Linden, A., Chauhan, S., Funke, B., Grabowski, U., Glatthor, N., Kiefer, M., Schieferdecker, T., Stiller, G.P., Versick, S.: Retrieval of temperature, H_2O, O_3, HNO_3, CH_4, N_2O, $ClONO_2$ and ClO from MIPAS reduced resolution nominal mode limb emission measurements. Atmos Meas Tech **2**, 159–175 (2009). doi:10.5194/amt-2-159-2009

Waugh, D.W., et al.: Mixing of polar vortex air into middle latitudes as revealed by tracer-tracer scatterplots. J Geophys Res **102**, 13,119–13,134 (1997)

Wrotny, J.E., Nedoluha, G.E., Boone, C., Stiller, G.P., McCormack, J.P.: Total hydrogen budget of the equatorial upper stratosphere. J Geophys Res **115**, D04302 (2010). doi:10.1029/2009JD012135